# Preprint: Torsion of a Cosserat Elastic Bar with Square Cross-Section: Theory and Experiment, Zeitschrift fur angewandte Mathematik und Physik (ZAMP), 69(2), 24 pages (2018).

W. J. Drugan and R. S. Lakes

University of Wisconsin-Madison
Department of Engineering Physics
1500 Engineering Drive
Madison, WI 53706, USA
drugan@engr.wisc.edu
lakes@engr.wisc.edu

March 10, 2020

**Abstract**

An approximate analytical solution for the displacement and microrotation vector fields is derived for pure torsion of a prismatic bar with square cross-section comprised of homogeneous, isotropic linear Cosserat elastic material. This is accomplished by analytical simplification coupled with use of the principle of minimum potential energy together with polynomial representations for the desired field components. Explicit approximate expressions are derived for cross-section warp and for applied torque versus angle of twist of the bar. These show that torsional rigidity exceeds the classical elasticity value, the difference being larger for slender bars, and that cross section warp is less than the classical amount. Experimental measurements on two sets of 3D printed square-cross-section polymeric bars, each set having a different microstructure and four different cross-section sizes, revealed size effects not captured by classical elasticity but consistent with the present analysis for physically sensible values of the Cosserat moduli. The warp can allow inference of Cosserat elastic constants independently of any sensitivity the material may have to dilatation gradients; warp also facilitates inference of Cosserat constants that are difficult to obtain via size effects.

# 1 Introduction

Solutions of boundary value problems are of use in the interpretation of experiments; they also reveal the physical meaning of elastic constants within a continuum theory. For example, an exact solution for torsion of a round rod of a Cosserat elastic solid is known [1]. Using this, one can obtain the Cosserat characteristic length for torsion by size effect tests on rods of different diameter, as was done for bone [3]. Similarly for bending, the exact solution for bending of a round Cosserat rod [2] may be used to interpret size effect measurements to extract the Cosserat characteristic length for bending. In principle, one may obtain all six isotropic Cosserat elastic constants from torsion and bending experiments. Such experiments have disclosed Cosserat effects in a dense isotropic foam and enabled determination of the six constants [4]. Bending, however, entails gradients of dilatation as well as gradients in rotation, so if the material exhibits any sensitivity to such gradients (as in void elasticity or micro-stretch elasticity), then one can no longer interpret effects in bending as due to Cosserat elasticity alone. Therefore alternative modalities are of interest. Torsion of a square section bar involves no gradients in dilatation and provides sensitivity to both characteristic lengths. Also, for many structured material types, fabrication of a bar with a round cross-section is not possible, and there are multiple applications in which the structural component has a square cross-section.

As no exact solution exists for torsion of a prismatic Cosserat elastic bar with square cross-section, we derive here an approximate solution that provides concise analytical expressions useful for characterization of torsion experiments on square bars comprised of materials whose response is not purely classically elastic. We confirm this utility by exhibiting excellent agreement of the new analytical results with recent experiments on two different 3D printed square polymeric lattice structures; this comparison shows that the lattice response is nonclassical but can be well-described by the Cosserat torsion results derived here, for physically sensible values of the Cosserat moduli that the comparison provides.

# 2 Theoretical Analysis

## 2.1 Full Governing Equations and Analytical Simplification

Here we derive an approximate solution to torsion of a homogeneous, isotropic, Cosserat linear elastic prismatic bar having a square cross section of side length $2a$.

The constitutive equations for an isotropic Cosserat [5] or micropolar [6] elastic solid are

$$\sigma_{ij} = 2G\epsilon_{ij} + \lambda\epsilon_{kk}\delta_{ij} + \kappa e_{ijk}(r_k - \phi_k) \tag{1}$$

$$m_{ij} = \alpha\phi_{k,k}\delta_{ij} + \beta\phi_{i,j} + \gamma\phi_{j,i} \tag{2}$$

in which $\sigma_{ij}$ is the force stress tensor (symmetric in classical elasticity but asymmetric here), $m_{ij}$ is the couple stress tensor (moment per unit area, asymmetric in general), $\epsilon_{ij} = (u_{i,j} + u_{j,i})/2$ is the (symmetric) small strain tensor, $u_i$ the displacement vector, and $e_{ijk}$ is the permutation symbol. The microrotation vector $\phi_i$ in Cosserat elasticity is kinematically distinct from the macrorotation vector $r_i = (e_{ijk}u_{k,j})/2$. $\phi_i$ refers to the rotation of points themselves, while $r_i$ refers to the rotation associated with movement of nearby points. The usual Einstein summation convention for repeated indices is employed, and a comma denotes differentiation with respect to ensuing subscripts, which represent Cartesian coordinates.

As Eqns. (1, 2) show, six independent elastic constants are required to describe general three-dimensional deformations of an isotropic Cosserat linear elastic solid: $\alpha$, $\beta$, $\gamma$, $\kappa$, $\lambda$ and $G$. (Eringen

[6] uses $2\mu + \kappa = 2G$, so $\mu$ differs from the shear modulus $G$ in his notation.) Classical elasticity is a special case, achieved by allowing $\alpha$, $\beta$, $\gamma$, $\kappa$ to become zero. The classical Lamé elastic constants $\lambda$ and $G$ then remain, and there is no couple stress. Technical constants are as follows:

$$\textit{Young's modulus} \qquad E = \frac{2G(3\lambda + 2G)}{2\lambda + 2G} \tag{3}$$

$$\textit{Shear modulus} \qquad G \tag{4}$$

$$\textit{Poisson's ratio} \qquad \nu = \frac{\lambda}{2(\lambda + G)} \tag{5}$$

$$\textit{Characteristic length, torsion} \qquad \ell = \sqrt{\frac{\beta + \gamma}{2G}} \tag{6}$$

$$\textit{Characteristic length, bending} \qquad \ell_b = \sqrt{\frac{\gamma}{4G}} \tag{7}$$

$$\textit{Coupling number} \qquad N = \sqrt{\frac{\kappa}{2G + \kappa}} \tag{8}$$

$$\textit{Polar ratio} \qquad \Psi = \frac{\beta + \gamma}{\alpha + \beta + \gamma}. \tag{9}$$

The complete governing equations for three-dimensional infinitesimal deformations of a homogeneous, isotropic linear elastic Cosserat medium in equilibrium when no body forces nor body couples act are the constitutive equations (1) and (2), the strain-displacement and macrorotation-displacement equations

$$\epsilon_{ij} = (u_{i,j} + u_{j,i})/2 \tag{10}$$

$$r_i = (e_{ijk} u_{k,j})/2, \tag{11}$$

and the equations of force and moment equilibrium, respectively

$$\sigma_{ij,i} = 0 \tag{12a}$$

$$m_{ij,i} + e_{jkl}\sigma_{kl} = 0. \tag{12b}$$

The force traction vector $t_i$ and the moment traction vector $m_i$ on a specimen's boundary are related through the boundary's outward unit normal vector $n_i$ to the force and couple stress tensors as

$$t_i = \sigma_{ji} n_j, \quad m_i = m_{ji} n_j. \tag{13}$$

Correct and complete boundary conditions require that at every point on the boundary's surface: the full displacement vector $\mathbf{u}$ *and* the full microrotation vector $\boldsymbol{\phi}$ are prescribed; or the full force traction vector $\mathbf{t}$ *and* the full moment traction vector $\mathbf{m}$ are prescribed; or some combination of these are prescribed so that at every surface point, two vector components from those just listed are prescribed in each of three independent directions, in such a way that one component of every term in the two sums appearing in the surface integral in Eq. (19) is prescribed; see e.g. Mindlin [7].

The six equilibrium governing field equations (12) can be expressed purely in terms of the displacement and microrotation components by substitution of Eq. (1, Eq. 2) using Eq. (10, Eq.

11); the resulting full set of governing equations is

$$(2G+\lambda)u_{x,xx} + (G+\frac{\kappa}{2})\,(u_{x,yy}+u_{x,zz}) + (G+\lambda-\frac{\kappa}{2})\,(u_{y,xy}+u_{z,xz}) + \kappa\,(\phi_{z,y}-\phi_{y,z}) = 0 \quad (14a)$$

$$(G-\frac{\kappa}{2}+\lambda)\,(u_{x,xy}+u_{z,yz}) + (G+\frac{\kappa}{2})\,(u_{y,xx}+u_{y,zz}) + (2G+\lambda)u_{y,yy} + \kappa\,(\phi_{x,z}-\phi_{z,x}) = 0 \quad (14b)$$

$$(G-\frac{\kappa}{2}+\lambda)\,(u_{x,xz}+u_{y,yz}) + (G+\frac{\kappa}{2})\,(u_{z,xx}+u_{z,yy}) + (2G+\lambda)u_{z,zz} + \kappa\,(\phi_{y,x}-\phi_{x,y}) = 0 \quad (14c)$$

$$(\alpha+\beta+\gamma)\phi_{x,xx} + (\alpha+\beta)\,(\phi_{y,xy}+\phi_{z,xz}) + \gamma\,(\phi_{x,yy}+\phi_{x,zz}) + \kappa\,(u_{z,y}-u_{y,z}-2\phi_x) = 0 \quad (14d)$$

$$(\alpha+\beta+\gamma)\phi_{y,yy} + (\alpha+\beta)\,(\phi_{x,xy}+\phi_{z,yz}) + \gamma\,(\phi_{y,xx}+\phi_{y,zz}) + \kappa\,(u_{x,z}-u_{z,x}-2\phi_y) = 0 \quad (14e)$$

$$(\alpha+\beta+\gamma)\phi_{z,zz} + (\alpha+\beta)\,(\phi_{x,xz}+\phi_{y,yz}) + \gamma\,(\phi_{z,xx}+\phi_{z,yy}) + \kappa\,(u_{y,x}-u_{x,y}-2\phi_z) = 0. \quad (14f)$$

For a prismatic bar of square cross-section with side length $2a$, Cartesian coordinates $x, y$ lie in the cross-section and $z$ is directed along the bar's centerline. We take the in-plane displacement components to have the classical linear elastic form, corresponding to rigid rotation of each cross-section of amount $\theta z$, where $\theta$ is angle of twist per unit length; symmetry requires $u_z = u_z(x,y)$, $\phi_x$=$\phi_x(x,y)$ and $\phi_y$=$\phi_y(x,y)$. Substituting these, Eq. (14a, b) require $\phi_z$ to be independent of $x, y$; both are then satisfied identically. Applying these restrictions, Eq. (14f) reduces to an ordinary differential equation for $\phi_z(z)$, whose exact particular solution is $\phi_z = \theta z$; its homogeneous solution must be discarded because it would produce purely $z$-dependent nonzero $\sigma_{xy}$ and $\sigma_{yx}$, which would violate the zero-traction boundary conditions on the bar's lateral surface. We have thus deduced that the solution form is

$$u_x = -\theta z y, \quad u_y = \theta z x, \quad \phi_z = \theta z, \quad u_z(x,y), \quad \phi_x(x,y), \quad \phi_y(x,y). \quad (15)$$

As noted, this solution form identically satisfies Equations (14a, b, f), leaving the three undetermined functions $u_z(x,y)$, $\phi_x(x,y)$ and $\phi_y(x,y)$ to be determined by simultaneous solution of the three remaining equations (14c, d, e), which simplify via application of Eq. (15) to:

$$(G+\frac{\kappa}{2})\,(u_{z,xx}+u_{z,yy}) + \kappa\,(\phi_{y,x}-\phi_{x,y}) = 0 \quad (16a)$$

$$(\alpha+\beta+\gamma)\phi_{x,xx} + (\alpha+\beta)\phi_{y,xy} + \gamma\phi_{x,yy} + \kappa\,(u_{z,y}-\theta x-2\phi_x) = 0 \quad (16b)$$

$$(\alpha+\beta+\gamma)\phi_{y,yy} + (\alpha+\beta)\phi_{x,xy} + \gamma\phi_{y,xx} - \kappa\,(u_{z,x}+\theta y+2\phi_y) = 0. \quad (16c)$$

The exact round bar solution of [1] also has the form Eq. (15), but in that simpler case, $u_z \equiv 0$, and the in-plane components of microrotation are more simply expressed as $\phi_r = \phi_r(r), \phi_\theta \equiv 0$.

The solution form Eq. (15), when substituted into Eqs. (10) and (11), corresponds to the vanishing of the following strain components and a specific expression for $r_z$:

$$\epsilon_{xx} = \epsilon_{yy} = \epsilon_{zz} = \epsilon_{xy} = \epsilon_{yx} = 0; \quad r_z = \theta z \quad \Longrightarrow \quad r_z - \phi_z = 0. \quad (17)$$

Employing these, Eqs. (1) and (2) show that the following stress and couple stress components are identically zero:

$$\sigma_{xx} = \sigma_{yy} = \sigma_{zz} = \sigma_{xy} = \sigma_{yx} = 0; \quad m_{xz} = m_{zx} = m_{yz} = m_{zy} = 0. \quad (18)$$

## 2.2 Approximate Solution via Principle of Minimum Potential Energy

We will employ the principle of minimum potential energy to determine an approximate solution for $u_z(x,y)$, $\phi_x(x,y)$ and $\phi_y(x,y)$. For a general three-dimensional body of homogeneous, isotropic, linear elastic Cosserat material contained in volume $V$ having surface $S$, the total potential energy is given by

$$\Pi = \int_V W dV - \int_{S_t} (t_i u_i + m_i \phi_i) dS, \tag{19}$$

where $S_t$ is the portion of $S$ on which force and/or moment tractions are prescribed, and

$$W = G\epsilon_{ij}\epsilon_{ij} + \frac{\lambda}{2}(\epsilon_{kk})^2 + \kappa(r_i - \phi_i)(r_i - \phi_i) + \frac{1}{2}\big[\alpha(\phi_{k,k})^2 + \beta\phi_{i,j}\phi_{j,i} + \gamma\phi_{i,j}\phi_{i,j}\big]. \tag{20}$$

Here is how we prescribe correct and complete boundary conditions in the present problem: On the bar ends, we prescribe $u_x, u_y, \phi_z$ to be as given in Eq. (15), and we prescribe $t_z = 0$ and $m_x = m_y = 0$ [these force-traction and couple-traction components are guaranteed to be zero on the bar ends due to Eq. (18)]. On the bar's lateral surfaces, we prescribe $\mathbf{t} = \mathbf{0}$ and $\mathbf{m} = \mathbf{0}$. Thus, everywhere on the bar's surface where force and/or moment tractions are prescribed, these are zero; therefore, the surface integral in Eq. (19) is identically zero.

Our approximate solution proceeds by assuming the following polynomial forms for the displacement and microrotation components that are not yet determined, where the $a$'s, $b$'s and $c$'s are undetermined constants:

$$u_z(x,y) = a_1 x^2 + a_2 xy + a_3 y^2 + ... + a_{25} y^6 \tag{21a}$$

$$\phi_x(x,y) = b_1 + b_2 x + b_3 y + ... + b_{21} y^5 \tag{21b}$$

$$\phi_y(x,y) = c_1 + c_2 x + c_3 y + ... + c_{21} y^5. \tag{21c}$$

Eq. (21a) is substituted into Eq. (10) and Eq. (11); the results and Eq. (21b, c) are then substituted into Eq. (20) to calculate the strain energy density $W$. Because this will be a function of $x, y$ only, the volume integral in (19) need only be evaluated over the cross-section of the bar; the result of this integration is then minimized with respect to all of the coefficients appearing in Eq. (21). This gives the optimal approximate solution according to the principle of minimum potential energy.

The potential energy minimization just explained shows that most of the coefficients in Eq. (21) vanish, and that several of the nonzero ones are related; renaming coefficients (the new ones are dimensionless), the solution forms for these quantities are found to be, where now and henceforth $x, y$ are nondimensionalized by the cross-section half side length $a$:

$$\frac{u_z(x,y)}{\theta a^2} = a_1(x^3 y - x y^3) + a_2(x^5 y - x y^5) \tag{22a}$$

$$\frac{\phi_x(x,y)}{\theta a} = b_1 x + b_2 x^3 + b_3 x y^2 + b_4 x^5 + b_5 x^3 y^2 + b_6 x y^4 \tag{22b}$$

$$\frac{\phi_y(x,y)}{\theta a} = b_1 y + b_3 x^2 y + b_2 y^3 + b_6 x^4 y + b_5 x^2 y^3 + b_4 y^5. \tag{22c}$$

The potential energy minimization gives the eight equations (A.1) of the Appendix for the eight coefficients in (22). In writing equations (A.1), we have employed Eq. (6, 7) to express the

results in terms of the characteristic lengths for torsion and bending, and we have then defined the dimensionless quantities:

$$\bar{\ell} = \frac{\ell}{a}, \quad \bar{\ell}_b = \frac{\ell_b}{a}, \quad \bar{\kappa} = \frac{\kappa}{G}, \quad \bar{\alpha} = \frac{\alpha}{a^2 G}. \tag{23}$$

It is clear from Eq. (A.1) that the full solutions for the coefficients are very lengthy.

From Eq. (A.1), the full solutions for the coefficients $a_1, a_2$ in terms of the other coefficients are:

$$a_1 = \frac{15 - \bar{\kappa}\left(15b_1 - 3b_2 + 15b_3 - 5b_4 + 5b_5 - b_6 + \frac{15}{2}\right)}{24(2+\bar{\kappa})} \tag{24a}$$

$$a_2 = \frac{33}{304}\frac{1 - \bar{\kappa}\left[b_1 + 3b_2 + b_3 + \frac{85}{33}b_4 + \frac{1}{10}(14b_5 + 42b_6 + 5)\right]}{2+\bar{\kappa}}. \tag{24b}$$

### 2.3 Explicit Results for Warping Displacement in Important Limiting Cases

As noted above, the full solutions for the coefficients $a_1, a_2$, and hence for the warping displacement $u_z$, are very lengthy. Here we give results for $u_z$ in some practically-important limiting cases in which it simplifies dramatically. In all results, $x$ and $y$ have been normalized by $a$, the bar half-width.

When $\bar{\kappa}$ and the $\bar{\ell}$'s are small, meaning that the coupling number $N$ is small, the full warping displacement expression Eq. (22a) reduces to:

$$\frac{u_z(x,y)}{\theta a^2/16} = 5\left(1 + \frac{21}{2}\frac{854\bar{\ell}^2 + 363\bar{\ell}_b^2}{D}\bar{\alpha}\bar{\kappa}\right)(x^3y - xy^3) + \frac{33}{38}\left(1 - \frac{105}{2}\frac{922\bar{\ell}^2 + 297\bar{\ell}_b^2}{D}\bar{\alpha}\bar{\kappa}\right)(x^5y - xy^5) \tag{25}$$

where

$$D = 266\bar{\alpha}\bar{\kappa} + 2\bar{\ell}^2\left[3255\bar{\alpha}(\bar{\kappa}+2) + 4259\bar{\kappa}\right] + 33\bar{\ell}_b^2\left[945\bar{\alpha}(1+\bar{\kappa}/2) + 499\bar{\kappa}\right]. \tag{26}$$

When the Cosserat moduli vanish, this reduces to the following classical approximate solution:

$$\frac{u_z(x,y)}{\theta a^2/16} = 5(x^3y - xy^3) + \frac{33}{38}(x^5y - xy^5). \tag{27}$$

More precisely, as is clear by inspection of Eq. (25) with Eq. (26), Eq. (25) reduces to Eq. (27) when either: (i) $\bar{\alpha} \to 0$; or (ii) $\bar{\kappa} \to 0$; or (iii) *both* $\bar{\ell} \to 0$ and $\bar{\ell}_b \to 0$. These same facts are true of the full solution for $u_z$ except that it does not reduce to Eq. (27) in the $\bar{\alpha} \to 0$ case when $\bar{\kappa}$ and the $\bar{\ell}$'s are not small.

Observe by comparison of Eq. (25) to Eq. (27) that Cosserat effects modify both the amplitude and the distribution of the cross-section's warp; when $\bar{\alpha} > 0$, this comparison shows Cosserat effects increase warp near the square cross-section center in the interior of the bar but decrease it on and near the cross-section edges. Also, examination of Eq. (25) with Eq. (26) shows that, speaking roughly since $D$ also depends on the $\bar{\ell}$'s, the effect of $\bar{\ell}$ on the warp is about a factor of 3 larger than that of $\bar{\ell}_b$.

The effect on warp in Eq. (25) is to reduce the peak warp on the surface; this effect increases with $\bar{\alpha}$ and decreases with $\bar{\ell}_b/\bar{\ell}$. The effect on warp is small in this regime: even for $\bar{\kappa} = 0.5$ and $\bar{\ell} = 0.5$, assuming $\bar{\alpha} = \bar{\ell}^2$ and $\bar{\ell}_b = 0.5\bar{\ell}$, the deviation of the warp from the classical curve (Eq. (27)) is only about 5% near the peak of the warp curve. If $\bar{\alpha} < 0$, which is allowed provided $\alpha$ is not too

negative, then the Cosserat effect on warp is reversed, so the peak warp can exceed the classical value. Observe that $\bar{\alpha} = 2\bar{\ell}^2(\Psi^{-1} - 1)$. The range [1] of $\Psi$ for stability is from 0 to 1.5.

For $\bar{\kappa} \to \infty$, corresponding to coupling number $N = 1$, the full warping displacement expression Eq. (22a) reduces to the following:

$$\frac{u_z(x,y)}{\theta a^2/16} = \frac{10\left(38 + 2211\bar{\ell}^2 + 2772\bar{\ell}_b^2\right)(x^3y - xy^3) + 33\left(2 - 315\bar{\ell}^2\right)(x^5y - xy^5)}{4\left(19 + 465\bar{\ell}^2 + 990\bar{\ell}^4\right) + 742.5\left(6 + 49\bar{\ell}^2\right)\bar{\ell}_b^2}. \tag{28}$$

In cases when the $\bar{\ell}$'s are small, neglecting their quartic terms compared to their quadratic ones in the denominator simplifies Eq. (28) to

$$\frac{u_z(x,y)}{\theta a^2/16} = 5\left(1 + 3\frac{854\bar{\ell}^2 + 363\bar{\ell}_b^2}{D_\infty}\right)(x^3y - xy^3) + \frac{33}{38}\left(1 - 15\frac{922\bar{\ell}^2 + 297\bar{\ell}_b^2}{D_\infty}\right)(x^5y - xy^5). \tag{29}$$

where

$$D_\infty = 4\left(19 + 465\bar{\ell}^2\right) + 4455\bar{\ell}_b^2. \tag{30}$$

The effects noted on warp by the Cosserat moduli in result Eq. (25) are clearly true here also, except that here the $\bar{\kappa} \to \infty$ limit has been taken, which also eliminates $\bar{\alpha}$ from the warp expression.

To illustrate graphically the effects of Cosserat elasticity, a range of elastic constants must be chosen. If the material has a positive definite strain energy, there are restrictions on the elastic constants. For classical elasticity, we have the familiar conditions that the shear modulus $G > 0$ and $(3\times)$ the bulk modulus $3\lambda + 2G > 0$. For Cosserat solids, additional restrictions apply [6]: $\kappa > 0$; $\gamma > 0$; $-\gamma < \beta < \gamma$; $3\alpha + \beta + \gamma > 0$. Regarding the bending characteristic length, $\gamma > 0$ implies $\ell_b > 0$. As for the relation between the characteristic lengths, at the upper limit $\frac{\beta}{\gamma} = 1$, $\ell_b = \frac{1}{2}\ell$; for $\frac{\beta}{\gamma} = 0$, $\ell_b = \frac{1}{\sqrt{2}}\ell$, and for $\frac{\beta}{\gamma} \to -1$, $\ell_b >> \ell$.

The effect of Cosserat elasticity on warp is shown for $N = 1$ in Fig. 1 by plotting Eq. (28). An increase in $\ell$ results in a reduction in warp on the cross-section boundary. The principal effects of $\ell_b$ are to change the shape of the warp curve, and also to further reduce the cross-section boundary warp. The shape effect is subtle particularly for small $\bar{\ell}$; substantial resolution would be required to discern it in an experiment.

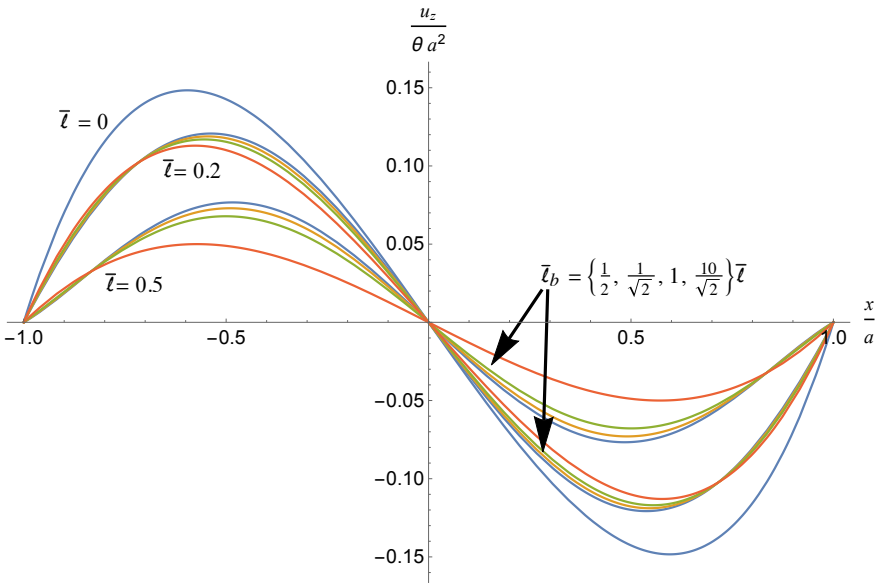


**Figure 1:** Warp of the cross-section edge $y = a$ for $N = 1$ and various $\bar{\ell}$, $\bar{\ell}_b$, from Eq. (28) (in which both $x, y$ are normalized by $a$). The classical elasticity warp curve is that labeled $\bar{\ell} = 0$.

The effect of various $N$ on warp for $\bar{\ell} = \bar{\ell}_b = 0.2$ based on the full solution is shown in Fig. 2. Larger values of $N$ are associated with a greater reduction in warp from classical values. When the characteristic length is larger, $\bar{\ell} = \bar{\ell}_b = 0.5$, as shown in Fig. 3, the warp is further reduced. Increasing $\bar{\alpha}$ increases (slightly) the warp provided $0 < N < 1$ but the effect of $\bar{\alpha}$ is small over the range considered.

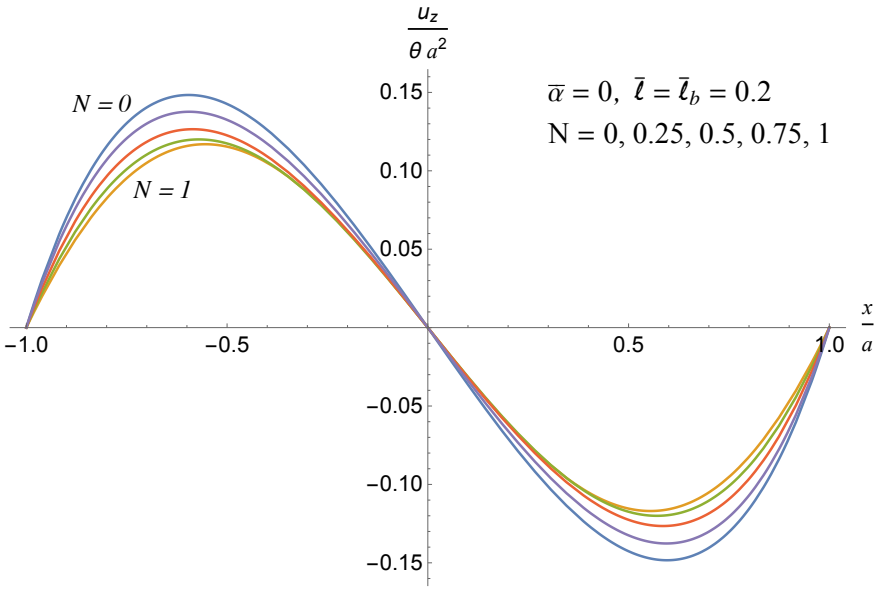


**Figure 2:** Warp of the cross-section edge $y = a$ for various $N$ and for $\bar{\ell} = \bar{\ell}_b = 0.2$, from the full solution (in which both $x, y$ are normalized by $a$).

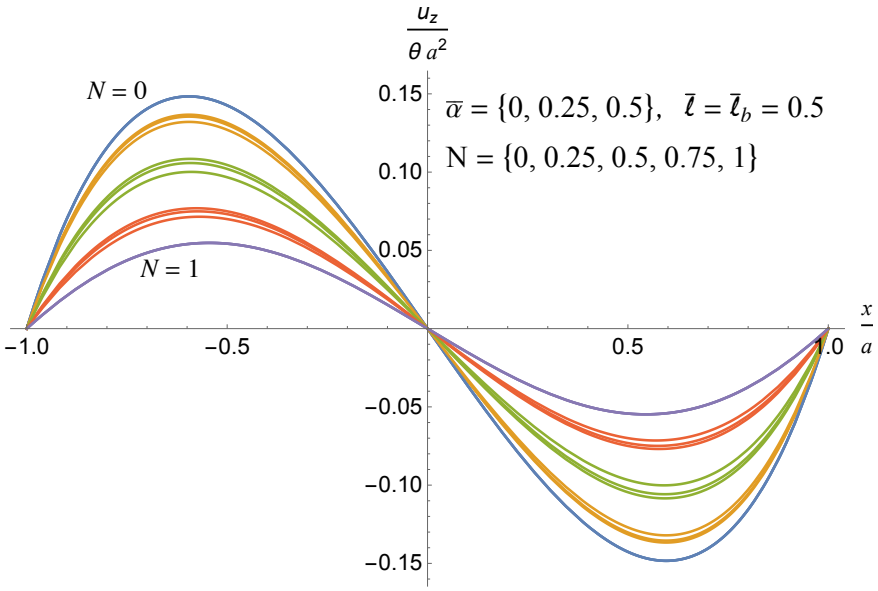


**Figure 3:** Warp of the cross-section edge $y = a$ for various $N$ and for $\bar{\ell} = \bar{\ell}_b = 0.5$, and for several $\bar{\alpha}$ from the full solution (in which both $x, y$ are normalized by $a$).

The overall effect of Cosserat elasticity is to reduce warp in comparison with the classical prediction. The warp reduction effect becomes more marked with an increase in $\bar{\ell}$ or with an increase in $N$. For large $N$, $\ell_b$ further reduces the warp and alters the shape of the warp curve. In the regime of small $\bar{\ell}$ and $N$ the warp deviates little from classical elasticity. In this regime, warp can increase above the classical value if $\bar{\alpha} < 0$. By contrast $\bar{\alpha}$ has no effect if $N = 1$.

## 2.4 Cosserat Effects on Total Torque

The total applied torque $T$ needed to produce an angle of twist per unit length $\theta$ is calculated as (where, recall, $x, y$ are normalized by $a$)

$$T = 4a^3 \int_0^1 \int_0^1 [x\sigma_{zy} - y\sigma_{zx} + m_{zz}]\, dxdy. \tag{31}$$

Employing the constitutive equations (1, 2) together with our solution forms, this evaluates to, in terms of the eight coefficients appearing in Eq. (22)

$$T = \frac{8}{3} G a^4 \theta \left[ \frac{1}{2}\left(2(1+3\bar{\ell}^2) + \bar{\kappa} + 3\bar{\alpha}\right) - (2-\bar{\kappa})\left(\frac{a_1}{5} + \frac{2}{7}a_2\right) + (3\bar{\alpha}+\bar{\kappa})\left(b_1 + \frac{b_3}{3} + \frac{b_6}{5}\right) \right.$$
$$\left. + (5\bar{\alpha}+\bar{\kappa})\left(\frac{3}{5}b_2 + \frac{b_5}{5}\right) + \frac{3}{7}(7\bar{\alpha}+\bar{\kappa})b_4 \right]. \tag{32}$$

Here are some explicit simplified results for the torque in important limiting cases. When $\bar{\kappa}$ is small (meaning that the coupling number $N$ is small) and the $\ell$'s are small, Eq. (32) reduces to:

$$T = \frac{898}{399} G a^4 \theta \left[ 1 + \frac{21\bar{\alpha}\bar{\kappa}(89\bar{\ell}^2 + \frac{363}{898}\bar{\ell}_b^2)}{266\bar{\alpha}\bar{\kappa} + 2\bar{\ell}^2[3255\bar{\alpha}(\bar{\kappa}+2) + 4259\bar{\kappa}] + 33\bar{\ell}_b^2[945\bar{\alpha}(1+\bar{\kappa}/2) + 499\bar{\kappa}]} \right]. \tag{33}$$

Observe from this that the approximation in the classical elasticity case – when the Cosserat moduli vanish – is

$$T = \frac{898}{399} G a^4 \theta. \tag{34}$$

This is a mere 0.05% higher than the exact value given by Timoshenko and Goodier [8]. More precisely, as is evident by inspection of Eq. (33), it reduces to Eq. (34) when either: (i) $\bar{\alpha} \to 0$; or (ii) $\bar{\kappa} \to 0$; or (iii) $\bar{\ell} \to 0$ *and* $\bar{\ell}_b \to 0$. Furthermore, Eq. (33) shows that when $\bar{\kappa}$ and the $\bar{\ell}$'s are small, and $\bar{\alpha} > 0$, Cosserat effects cause an increase in torsional rigidity. Result Eq. (33) also shows that in this small parameter regime, the effects of $\bar{\ell}_b$ on the torsional rigidity are essentially negligible (two orders of magnitude smaller) compared to those of $\bar{\ell}$.

When $\kappa \to \infty$, which corresponds to the coupling number $N = 1$, the total torque expression simplifies to

$$T = \frac{4}{21} G a^4 \theta \frac{1796 + 126\left(449 + 2740\bar{\ell}^2 + 3960\bar{\ell}^4\right)\bar{\ell}^2 + 693\left(152 + 2280\bar{\ell}^2 + 6615\bar{\ell}^4\right)\bar{\ell}_b^2}{8\left(19 + 465\bar{\ell}^2 + 990\bar{\ell}^4\right) + 1485\left(6 + 49\bar{\ell}^2\right)\bar{\ell}_b^2}. \tag{35}$$

Observe that the result is independent of $\bar{\alpha}$. When the $\bar{\ell}$'s are small, retaining only terms through second order in them in the numerator and denominator simplifies Eq. (35) to:

$$T = \frac{898}{399} G a^4 \theta \left[1 + \frac{267}{898} \frac{449\bar{\ell}^2 + \frac{363}{178}\bar{\ell}_b^2}{19 + 465\bar{\ell}^2 + \frac{4455}{4}\bar{\ell}_b^2}\right]. \tag{36}$$

Clearly, conclusions drawn in the small $\bar{\kappa}$ case are true here as well: Eq. (36) reduces to the classical approximate result Eq. (34) when $\bar{\ell} \to 0$ *and* $\bar{\ell}_b \to 0$; Cosserat effects produce an increase in torsional rigidity; and the effects on torsional rigidity of $\bar{\ell}_b$ are negligible compared to those of $\bar{\ell}$.

The effect of Cosserat elasticity on rigidity is illustrated in Fig. 4 by plotting the full torque solution for the case $N = 0.5, \Psi = 0$. Slender specimens become stiffer than expected classically, as is the case for circular cylinders. Increasing $\ell$ results in increasing torsional rigidity. Observe that the full solution shows in this case what the explicit small and large $\bar{\kappa}$ solutions just derived show analytically: $\ell_b$ has negligible effect on torsional rigidity compared to that of $\ell$. Fig. 5 shows the effect of varying $N$ for $\Psi = 1.5$ and for $\Psi = 1.0$. For $\Psi = 1.5$ the effect of $N$ is evident in the size effects, but not for $\Psi = 1.0$. This behavior is similar to that of round rods: size effects depend on $\ell$, $N$ and $\Psi$, but the sensitivity to parameter changes is not uniform; the effect of $N$ is substantial only for large $\Psi$ at or near its upper limit 1.5.

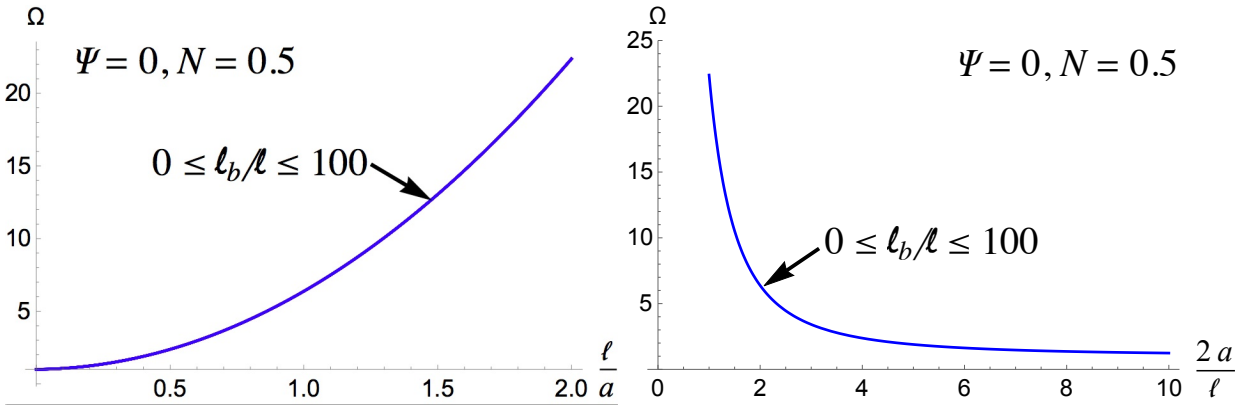


**Figure 4:** Size effect for $N = 0.5$ and $\Psi = 0$ as a function of $\ell/a$, plotted two ways. Here, $\Omega$ is the torsional rigidity $T/\theta$ normalized by its classical elasticity approximate value: $\Omega = \frac{T}{\theta} / \left(\frac{898}{399} G a^4\right)$, so that $\Omega = 1$ in the absence of Cosserat effects ($\ell = 0$).

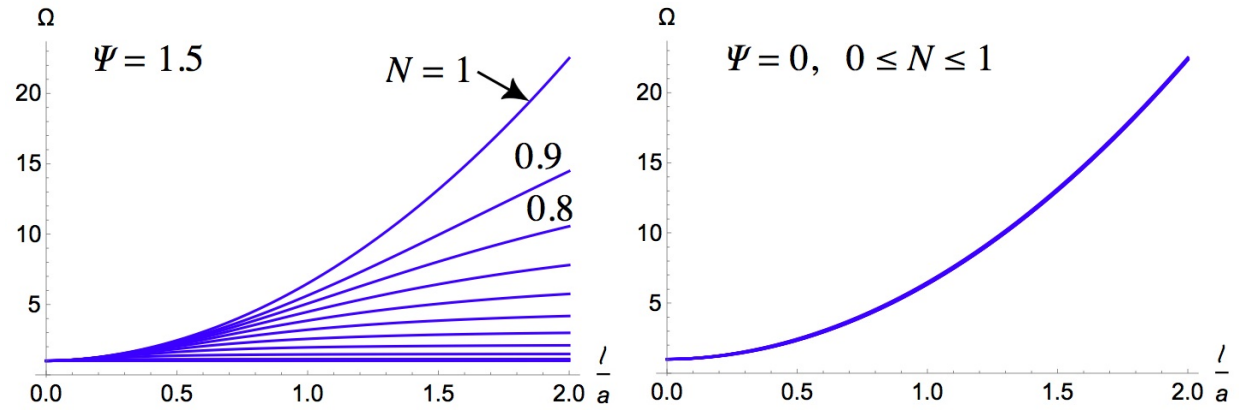


**Figure 5:** Left, size effect for $\Psi = 1.5$ and various $N$, as a function of $\ell/a$. Right, size effect for $\Psi = 1.0$ and various $N$, as a function of $\ell/a$. $\Omega$ is the torsional rigidity $T/\theta$ normalized by its classical elasticity approximate value: $\Omega = \frac{T}{\theta} / \left(\frac{898}{399} G a^4\right)$, so that $\Omega = 1$ in the absence of Cosserat effects ($\ell = 0$).

## 3 Comparison with Experimental Results

Several lattices were examined for size effects. Each lattice was a polymeric structure prepared via 3D printing. Lattices differ from foams in that they are prepared with the desired shape. There is no cutting or machining therefore no damaged or incomplete cells which can result in an underestimate of characteristic length. Bar specimens were made with the same structure but different overall size and with a square cross section. Size dependence of rigidity was determined via broadband viscoelastic spectroscopy upon specimens of different thickness. This method allows torsion and bending studies upon the same specimen with zero parasitic error due to friction. Mechanical damping is readily measured but is not the focus of the study.

Bars comprised of a negative Poisson's ratio lattice (inset in Fig. 6) with tetragonal symmetry were tested. Details regarding this lattice and the measurements are reported elsewhere [9]. The cell size in the transverse direction is about 15 mm. A fit of the theoretical relative stiffness result

obtained in Eq. (35) to experimental size effect results for the negative Poisson's ratio lattice are shown in Fig. 6. The lattice exhibits a negative Poisson's ratio combined with relatively high stiffness [10]. The inferred shear modulus is $G = 0.67$ MPa, the coupling number $N = 1$, and $\ell = 5.6$ mm, $\ell_b = 5.4$ mm; the goodness of fit is $R^2 = 0.999$. The lattice is anisotropic, so the elastic constants are interpreted as technical constants, not tensorial ones. Anisotropy cannot be a confounding variable because there are no size effects in anisotropic classical elasticity. A value of $N$ at or near its upper limit of 1 is sensible for lattices in which rib deformation is bend dominated. For example, a 2-D chiral negative Poisson's ratio honeycomb lattice [12] analyzed as a Cosserat solid had a Cosserat coupling number $N$ approaching 1 [13]. Similarly, experiments on small cell polymer foam disclosed $N \approx 1$ [14]. By contrast, lattices with straight ribs [15] in a fully stretch dominated mode are predicted to have $N << 1$ and $\ell$ much smaller than the cell size, hence very weak effects are predicted.

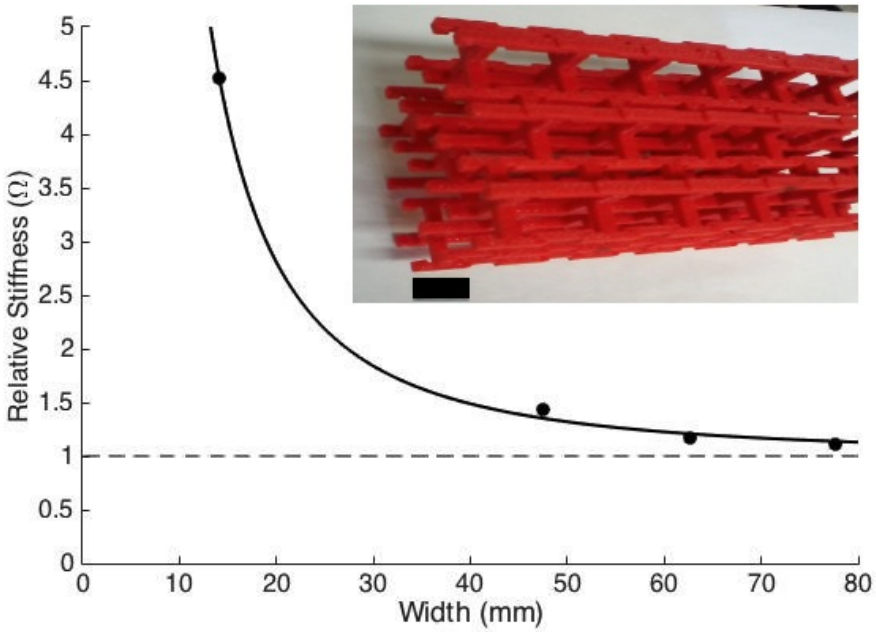


**Figure 6:** Size effects in bars of square cross-section comprised of a tetragonal lattice (inset; the scale bar is 1 cm). The points are the experimental values reported in [9], the solid curve is the best Cosserat fit to them from Eq. (35); $\Omega$ is the torsional rigidity $T/\theta$ normalized by its classical elasticity approximate value: $\Omega = \frac{T}{\theta} / \left(\frac{898}{399} G a^4\right)$, so that $\Omega = 1$ in the absence of Cosserat effects ($\bar{\ell} = \bar{\ell}_b = 0$) as indicated by the horizontal dashed line.

Bars of square cross section comprised of a lattice of cubic cells of width 13 mm were also tested [11], Fig. 7. The experimental data were again best-fit to Eq. (35), since a coupling number $N \approx 1$ is also expected for this microstructure. The inferred moduli are: shear modulus $G = 4.2$ MPa, and $\ell = 3.8$ mm, $\ell_b = 3.8$ mm; the goodness of fit is $R^2 = 0.86$. This material is stiffer than the tetragonal lattice. Rib extension is therefore more prominent than rib bending in comparison with the tetragonal lattice. That difference is the likely cause of the smaller characteristic length and smaller size effects. The dip in the experimental points was a matter of concern, therefore all size effect measurements were repeated, with no change in the inference. The lattices were examined visually but no obvious defect or damage was observed. The non-monotonic size dependence is attributed to imperfection in the 3D printing process.

For these lattices the inferred Cosserat parameters are reasonable in view of the facts that bending of structural elements is likely to contribute substantially to the deformation but the lattices are not optimized for Cosserat elasticity.

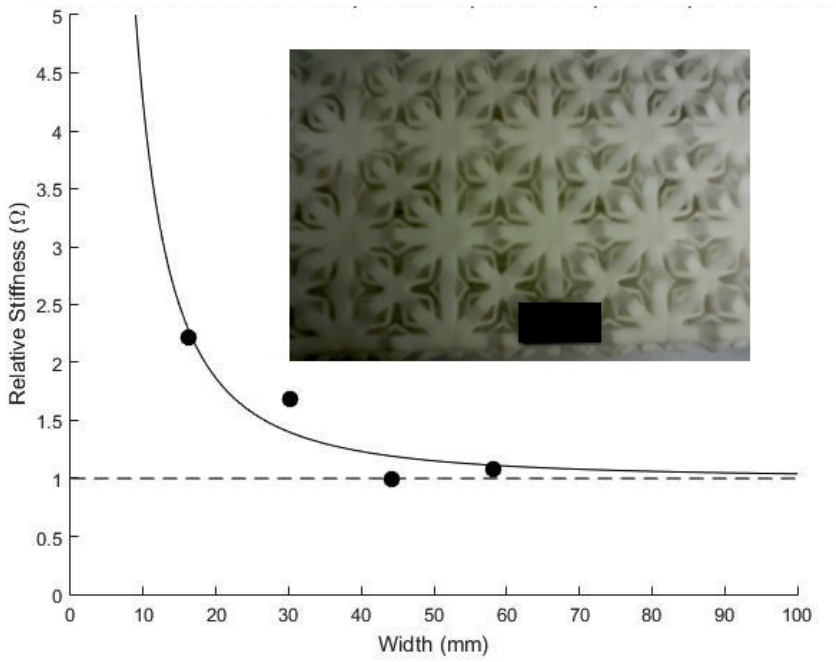


**Figure 7:** Size effects in bars of square cross section comprised of a cubic lattice (inset; the scale bar is 1 cm). The points are experimental values; the solid curve is our approximate Cosserat solution Eq. (35) best-fit to them. The horizontal dashed line is the classical elasticity solution.

# 4 Discussion

As with rods of circular cross section [1], size effects are predicted in which slender square section bars have a higher structural rigidity than is predicted classically; the difference increases as bar width decreases. Size effects depend primarily on $\ell$, not perceptibly on $\ell_b$, as shown explicitly in Eqs. (33) and (36) and illustrated in Fig. 4. The magnitude of the warp of the cross section edges decreases as $\ell$ increases and as $N$ increases. Warp of the cross-section edges also decreases with $\ell_b$, and the shape of the warp curve varies with $\ell_b$.

As for other solutions, the analysis of torsion of a round bar [1] has been discussed above. The general problem of torsion in micropolar beams of arbitrary cross section shape has been formulated in [16], where it was shown that if the three-dimensional displacement and microrotation fields are assumed to have the forms we have deduced here in Eq. (15), torsion of a micropolar beam of arbitrary cross section can be reduced to a Neumann boundary value problem in antiplane micropolar elasticity. A numerical solution for a graphite rod of square cross section was presented in [17]. An approximation for square cross section done via a semi inverse approach [18] is similar to the present results in the regime of small $\bar{\kappa}$. It is restricted to a range of $\beta/\gamma$ between 0 and 0.6 (hence a restricted range of $\ell_b$); size effect predictions for large $N$ are similar to the present results

but warp reduction is overestimated. The present approach therefore provides superior results.

The present results enable an enhanced experimental paradigm for determining Cosserat elastic constants. One may conduct torsional stiffness size effect experiments on specimens of round or square cross section to reveal $\ell$; knowing this, one may then conduct a warp experiment on a bar of square cross section, from which $N$ may be inferred. If resolution in the warp measurement suffices, one may obtain $\ell_b$ as well from the shape of the warp curve. In the present experiments, lattices had sufficiently many cells for size effects but not for warp; specimens with more cells would be needed. The rationale is as follows. One can in principle obtain all the Cosserat elastic constants from torsion and bending size effect studies on round specimens. In practice, the rigidity is not uniformly sensitive to variation in the constants over their ranges. In particular, torsional rigidity of a round rod in the range $\Psi$ from 0 to 1 shows strong size effects with no roll off of rigidity for small radius. In this part of the range, the stiffening can be large even for small $N$. Roll off of rigidity to a finite value for small radius occurs in the round case if $\Psi = 1.5$ which entails $\alpha$ at its lower (negative) limit; similar behavior is predicted in the square case. In summary, warp studies are revealing because the role of $N$ in the warp effect is very prominent in comparison with its role in in size effects unless $\Psi = 1.5$.

These results provide the potential for new experimental modalities that are insensitive to gradients of dilatation; if the material obeys micro-stretch elasticity [19] then it is sensitive to gradients of rotation as in Cosserat elasticity as well as to gradients in dilatation. Bending experiments entail gradients of both rotation and dilatation so they reveal $\ell_b$ unambiguously only if the material is known to be a Cosserat solid without sensitivity to dilatation. If all the experiments are done in torsion, any hypothetical sensitivity to dilatation gradient cannot obtrude in the interpretation because there is no dilatation in torsion. By contrast, bending entails gradients both in rotation and in dilatation so if the material is sensitive to such gradients, interpretation of experiments becomes much more challenging.

As for $\alpha$, torsion in both the round and square cases reveals sensitivity to $\alpha$ but bending of plates [1] and of round rods [2] is insensitive to $\alpha$. Because $\alpha$ provides sensitivity to the trace of the rotation gradient, it appears in torsion analyses because the gradient in the axial direction is forced by torsion, and the gradients in the transverse direction are forced by the requirement that couple stress corresponding to these gradients is forced to zero at the free surfaces.

Strain distribution in the bar is related to warp. The surface shear strain in a classical elastic square cross section bar is maximum at the center of each lateral surface and zero at the edges. Reduced warp associated with Cosserat elasticity implies a reduction of maximum strain and redistribution of strain to the edges. This reduction of strain concentration may be beneficial in enhancing toughness.

## 5 Conclusion

The present analysis of torsion of a square cross section Cosserat elastic bar reveals size effects in which slender bars are more rigid than expected classically. Size effects increase with the torsion characteristic length $\ell$ and the coupling number $N$; there is negligible sensitivity to $\ell_b$ in comparison to the case of a round cross section in which there is zero sensitivity to $\ell_b$. Warp of cross sections is reduced compared with a classical solid. Warp reduction increases with $\ell$ and $N$; to a lesser extent with $\ell_b$. The shape of the warp curve depends on $\ell_b$. These sensitivities can form the basis of new experimental approaches that are insensitive to dilatation gradients that may occur if the material has such freedom as well as the Cosserat freedom. The warp analysis can reveal Cosserat elastic constants such as $N$ which may be difficult to infer via size effects.

## Acknowledgments

Support of the National Science Foundation under Grant CMMI-1361832 is gratefully acknowledged.

## References

[1] Gauthier, R. D. and W. E. Jahsman, A quest for micropolar elastic constants. J. Applied Mechanics, **42**, 369-374 (1975).
[2] Krishna Reddy, G. V. and Venkatasubramanian, N. K., On the flexural rigidity of a micropolar elastic circular cylinder, J. Applied Mechanics **45**, 429-431 (1978).
[3] Yang, J. F. C. and Lakes, R. S., Transient study of couple stress in compact bone: torsion, Journal of Biomechanical Engineering, 103, 275-279, (1981).
[4] Lakes, R. S., Experimental microelasticity of two porous solids, Int. J. Solids and Structures, **22**, 55-63 (1986).
[5] Cosserat, E. and Cosserat, F., *Theorie des Corps Deformables*, Hermann et Fils, Paris (1909).
[6] Eringen, A.C., Theory of micropolar elasticity. In *Fracture* **1**, 621-729 (edited by H. Liebowitz), Academic Press, New York (1968).
[7] Mindlin, R. D., Stress functions for a Cosserat continuum, Int. J. Solids Structures **1**, 265-271 (1965)
[8] Timoshenko, S. and Goodier, J. N., *Theory of Elasticity*, McGraw-Hill, New York (1970)
[9] Rueger, Z., Li, D. and Lakes, R. S., Observation of Cosserat elastic effects in a tetragonal negative Poisson's ratio lattice, Physica Status Solidi B: Basic Solid State Physics 1600840, 6 pages, Oct. (2017).
[10] Li, D., Ma, J., Dong, L. Lakes, R. S., Three-dimensional stiff cellular structures with negative Poisson's ratio, Physica Status Solidi B: Basic Solid State Physics 1600785, 5 pages, (2017). DOI: 10.1002/pssb.201600785
[11] Rueger, Z. and Lakes, R. S, Cosserat elasticity in lattices, in preparation.
[12] Prall, D. and Lakes, R. S., Properties of a chiral honeycomb with a Poisson's ratio -1, Int. J. of Mechanical Sciences, 39, 305-314, (1997).
[13] Spadoni, A. and Ruzzene, M. Elasto-static micropolar behavior of a chiral auxetic lattice, J. Mechs Physics of Solids, **60**, 156-171 (2012).
[14] Rueger, Z. and R. S. Lakes, Experimental Cosserat elasticity in open cell polymer foam, Philosophical Magazine, **96**, 93-111 (2016).
[15] Askar A. and Cakmak, A. S., A structural model of a micropolar continuum, Int. J. Engng. Sci. **6**, 583-589 (1968).
[16] Iesan D. Torsion of micropolar elastic beams. Int. J. Engng. Sci. 9, 1047-1060 (1971).
[17] Shmoylova E., Potapenko S., Dorfmann A. Weak solutions to anti-plane boundary value problems in a linear theory of elasticity with microstructure. Arch. Mech., 59(6), 519-539 (2007) .
[18] Park, H. C. and Lakes, R. S. Torsion of a micropolar elastic prism of square cross section, Int. J. Solids, Structures, 23, 485-503 (1987).
[19] Eringen, A. C. Theory of thermo-microstretch elastic solids, Int. J. Engng. Sci., **28** (12) 1291-1301, (1990).

# Appendix

The potential energy minimization explained in Section 2.2 gives the following eight equations for the eight coefficients in Eq. (22). The interested reader, by employing e.g. Mathematica to solve Eq. (A.1) and then using the results in Eq. (22), will have the full approximate solution employed in this paper. [Provision of (A.1) is the most concise way to report the full approximate solution; the solution to Eq. (A.1) is far more lengthy.]

$$
\begin{pmatrix}
135(2+\bar{\kappa}) & 190(2+\bar{\kappa}) & 105\bar{\kappa} & 45\bar{\kappa} & 105\bar{\kappa} \\
627(2+\bar{\kappa}) & 950(2+\bar{\kappa}) & 495\bar{\kappa} & 231\bar{\kappa} & 495\bar{\kappa} \\
21\bar{\kappa} & 30\bar{\kappa} & 105\left(\bar{\kappa}+3\bar{\ell}^2+3\bar{\alpha}\right) & 63\left(\bar{\kappa}+5\bar{\ell}^2+5\bar{\alpha}\right) & 35\left(\bar{\kappa}+3\bar{\ell}^2+3\bar{\alpha}\right) \\
45\bar{\kappa} & 70\bar{\kappa} & 315\left(\bar{\kappa}+5\bar{\ell}^2+5\bar{\alpha}\right) & 45\left(5\bar{\kappa}+63\bar{\ell}^2+49\bar{\alpha}\right) & 105\left(\bar{\kappa}+5\bar{\ell}^2+7\bar{\alpha}\right) \\
105\bar{\kappa} & 150\bar{\kappa} & 175\left(\bar{\kappa}+3\bar{\ell}^2+3\bar{\alpha}\right) & 105\left(\bar{\kappa}+5\bar{\ell}^2+7\bar{\alpha}\right) & 35\left(3\bar{\kappa}+29\bar{\ell}^2+7\bar{\alpha}\right) \\
165\bar{\kappa} & 270\bar{\kappa} & 1485\left(\bar{\kappa}+7\bar{\ell}^2+7\bar{\alpha}\right) & 165\left(7\bar{\kappa}+135\bar{\ell}^2+99\bar{\alpha}\right) & 495\left(\bar{\kappa}+7\bar{\ell}^2+11\bar{\alpha}\right) \\
171\bar{\kappa} & 250\bar{\kappa} & 315\left(\bar{\kappa}+5\bar{\ell}^2+5\bar{\alpha}\right) & 45\left(5\bar{\kappa}+63\left(\bar{\ell}^2+\bar{\alpha}\right)\right) & 63\left(3\bar{\kappa}+35\bar{\ell}^2+15\bar{\alpha}\right) \\
243\bar{\kappa} & 370\bar{\kappa} & 315\left(\bar{\kappa}+3\bar{\ell}^2+3\bar{\alpha}\right) & 27\left(7\bar{\kappa}+35\bar{\ell}^2+55\bar{\alpha}\right) & 45\left(5\bar{\kappa}+71\bar{\ell}^2+11\bar{\alpha}\right)
\end{pmatrix}
$$

$$
\begin{pmatrix}
25\bar{\kappa} & 57\bar{\kappa} & 81\bar{\kappa} \\
135\bar{\kappa} & 275\bar{\kappa} & 407\bar{\kappa} \\
45\left(\bar{\kappa}+7\bar{\ell}^2+7\bar{\alpha}\right) & 21\left(\bar{\kappa}+5\bar{\ell}^2+5\bar{\alpha}\right) & 21\left(\bar{\kappa}+3\bar{\ell}^2+3\bar{\alpha}\right) \\
25\left(7\bar{\kappa}+135\bar{\ell}^2+99\bar{\alpha}\right) & 15\left(5\bar{\kappa}+63\left(\bar{\ell}^2+\bar{\alpha}\right)\right) & 9\left(7\bar{\kappa}+35\bar{\ell}^2+55\bar{\alpha}\right) \\
75\left(\bar{\kappa}+7\bar{\ell}^2+11\bar{\alpha}\right) & 21\left(3\bar{\kappa}+35\bar{\ell}^2+15\bar{\alpha}\right) & 15\left(5\bar{\kappa}+71\bar{\ell}^2+11\bar{\alpha}\right) \\
105\left(9\bar{\kappa}+275\bar{\ell}^2+187\bar{\alpha}\right) & 385\bar{\kappa}+7425\left(\bar{\ell}^2+\bar{\alpha}\right) & 33\left(9\bar{\kappa}+63\bar{\ell}^2+119\bar{\alpha}\right) \\
175\bar{\kappa}+3375\left(\bar{\ell}^2+\bar{\alpha}\right) & 9\left(15\bar{\kappa}+273\bar{\ell}^2+32\bar{\ell}_b^2+189\bar{\alpha}\right) & 9\left(15\bar{\kappa}+275\bar{\ell}^2-64\bar{\ell}_b^2+75\bar{\alpha}\right) \\
15\left(9\bar{\kappa}+63\bar{\ell}^2+119\bar{\alpha}\right) & 9\left(15\bar{\kappa}+275\bar{\ell}^2-64\bar{\ell}_b^2+75\bar{\alpha}\right) & 175\bar{\kappa}+3549\bar{\ell}^2+1152\bar{\ell}_b^2+357\bar{\alpha}
\end{pmatrix}
\begin{pmatrix} a_1 \\ a_2 \\ b_1 \\ b_2 \\ b_3 \\ b_4 \\ b_5 \\ b_6 \end{pmatrix}
$$

$$
= -\frac{5}{2}
\begin{pmatrix}
21(\bar{\kappa}-2) \\
99(\bar{\kappa}-2) \\
21\left(\bar{\kappa}+3\bar{\alpha}\right) \\
63\left(\bar{\kappa}+5\bar{\alpha}\right) \\
35\left(\bar{\kappa}+3\bar{\alpha}\right) \\
297\left(\bar{\kappa}+7\bar{\alpha}\right) \\
63\left(\bar{\kappa}+5\bar{\alpha}\right) \\
63\left(\bar{\kappa}+3\bar{\alpha}\right)
\end{pmatrix}
. \quad \text{(A.1)}
$$